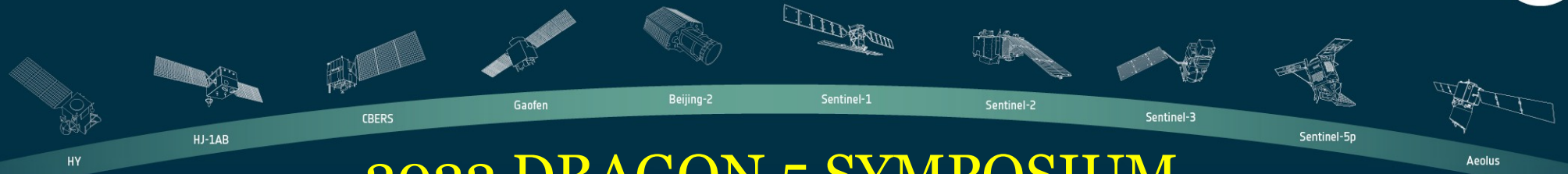

2022 DRAGON 5 SYMPOSIUM

MID-TERM RESULTS REPORTING

17-21 OCTOBER 2022

PROJECT ID. 59307

3-D CHARACTERIZATION AND TEMPORAL ANALYSIS OF VEGETATED AREAS USING TIME-SERIES OF POLARIMETRIC SAR DATA AND TOMOGRAPHIC PROCESSING

2022/10/22

ID. 59307

3-D CHARACTERIZATION AND TEMPORAL ANALYSIS OF VEGETATED AREAS USING TIME-SERIES OF POLARIMETRIC SAR DATA AND TOMOGRAPHIC PROCESSING

PRINCIPAL INVESTIGATORS:

E. CHEN (CAF & IFRIT), L. FERRO-FAMIL (ISAE-SUPAERO & CESBIO (FR))

CO-AUTHORS:

E. POTTIER, Z. LI, T. LE TOAN, W. HONG, X. LI, Q. YIN

PRESENTED BY: L. FERRO-FAMIL

3-D CHARACTERIZATION AND TEMPORAL ANALYSIS OF VEGETATED AREAS USING TIME-SERIES OF POLARIMETRIC SAR DATA AND TOMOGRAPHIC PROCESSING

WP 1: 3-D characterization of forested and vegetated areas using low-frequency PolSAR/ PolInSAR/ PolTomoSAR data

- WP 1-1: 3-D characterization of forested areas using low-frequency SAR tomography technology
- WP 1-2: Synergies of low-frequency (L-, P- band) and high-frequency (X-, C- band) SAR data for characterization of forested and vegetated areas
- WP 1-3: Requirement analysis and feasibility demonstration for China's P-band SAR satellite
- WP 1-4: Simulation of spaceborne data sets and adaption of the developed techniques to the corresponding specific configurations

3-D CHARACTERIZATION AND TEMPORAL ANALYSIS OF VEGETATED AREAS USING TIME-SERIES OF POLARIMETRIC SAR DATA AND TOMOGRAPHIC PROCESSING

WP 2: Innovative 3-D imaging modes and techniques

- WP 2-1: Tandem-like PolTomSAR (at L- (Tandem-L) or C-(S1-CS) bands) for forest and agricultural volume imaging
- WP 2-2: Bistatic tomography (Companion Satellite) for improved SNR and vertical imaging potential
- WP 2-3: Wavelet-Based CS imaging and other innovative techniques for vegetated area characterization

3-D CHARACTERIZATION AND TEMPORAL ANALYSIS OF VEGETATED AREAS USING TIME-SERIES OF POLARIMETRIC SAR DATA AND TOMOGRAPHIC PROCESSING

WP 3: Temporal monitoring of forested and vegetated areas using time-series of acquisitions

- WP 3-1: Forest and grassland disaster monitoring from multi-temporal PolSAR and PolinSAR features/descriptors using high-level detection and classification techniques (Airborne sensors, ALOS)
- WP 3-2: Woody Savannah AGB estimation (Tropics), mapping (S America+ Africa+ Australia) and deforestation rate (Cambodia) using ALOS time -seris
- WP 3-3: Nearly real-time deforestation mapping (Tropics and S. America), temperate (France) forest parameter mapping using S1 time series

WP 4: PolSARpro Software continued development.

Method

Overall network structure

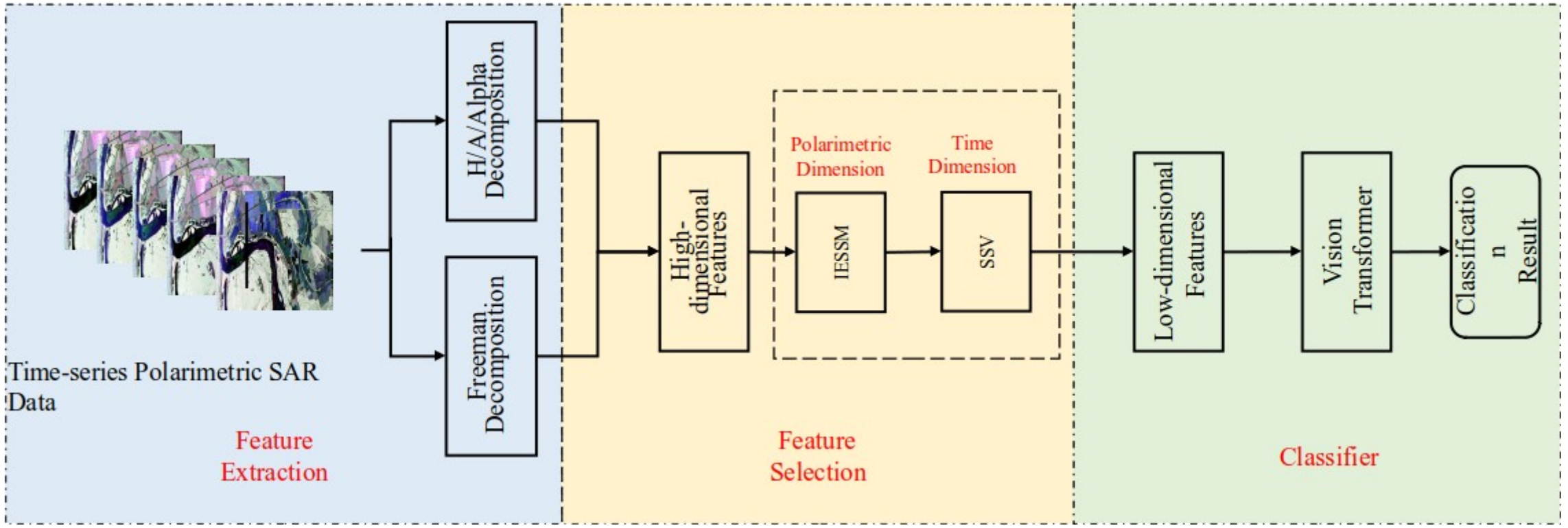

Polarization decomposition of the pre-processed time-series polarimetric SAR image

For the decomposed high-dimensional features, feature selection is performed from polarization and time dimensions.

Verification of feature selection results by Vision Transformer

Beijing University of Chemical Technology (BUCT), Q. Yin

Experiment and conclusions

Data

This paper uses the data of UAVSAR for experiments. It includes 5 Fully-PolSAR images from July 1, 2019 to September 23, 2019. It contains 16 categories, and the labeling area has a total of 9047044 pixels.

2019-07-01

2019-07-16

2019-07-25

2019-08-12

2019-09-23

Ground Truth

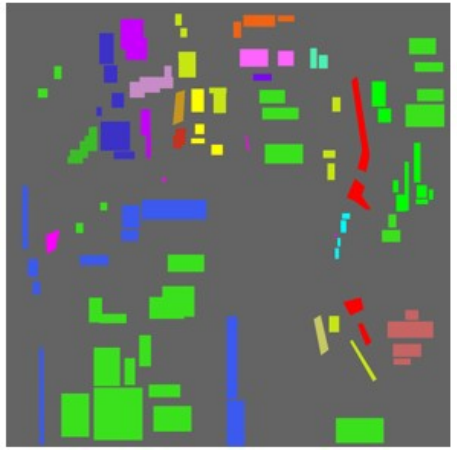

Experiment and conclusions

Young Scientist Poster id: 135

Features	IESSM	SSV	IESSM+SSV
Alpha	0.8995	0.2661	**1.1656**
Anisotropy	0.9171	0.5520	1.4691
Beta	0.9077	0.4850	**1.3927**
(1-H)(1-A)	0.8563	0.3491	**1.2054**
(1-H)A	0.7893	0.4473	**1.2312**
H(1-A)	0.8961	0.4971	**1.3932**
HA	0.9223	0.4925	1.4148
Delta	0.9137	0.5090	1.4227
Entropy	0.8532	0.3510	**1.2042**
Gamma	0.9176	0.7269	1.6445
Lambda	0.9084	0.2603	**1.1687**
Freeman_Dbl	0.8730	0.3831	**1.2561**
Freeman_Odd	0.8642	0.5951	1.4593
Freeman_Vol	0.8922	0.2275	**1.1197**

Method	Accuracy
ResNet-14+all 14 features	86.68%
Vision Transformer +all 14 features	**88.02%**
ResNet-14+9 features	85.99%
Vision Transformer +9 features	**87.38%**

We selected nine outstanding features based on the proposed feature selection method and conducted related experiments on ResNet with Vision Transformer, and the results proved t-he effectiveness of Vision Transformer. Our selected features also achieve essentially equal accuracy compared to all featu-res.

*Zhiyuan Lin, Jiaxin Cui, Qiang Yin et.al. Time-series PolSAR crop Classification based on joint feature extraction (IGARSS2022(EI),Oral)

A new approach for forest height inversion using X-band single-pass InSAR coherence

Coherence estimation from InSAR data should be consistent with the model

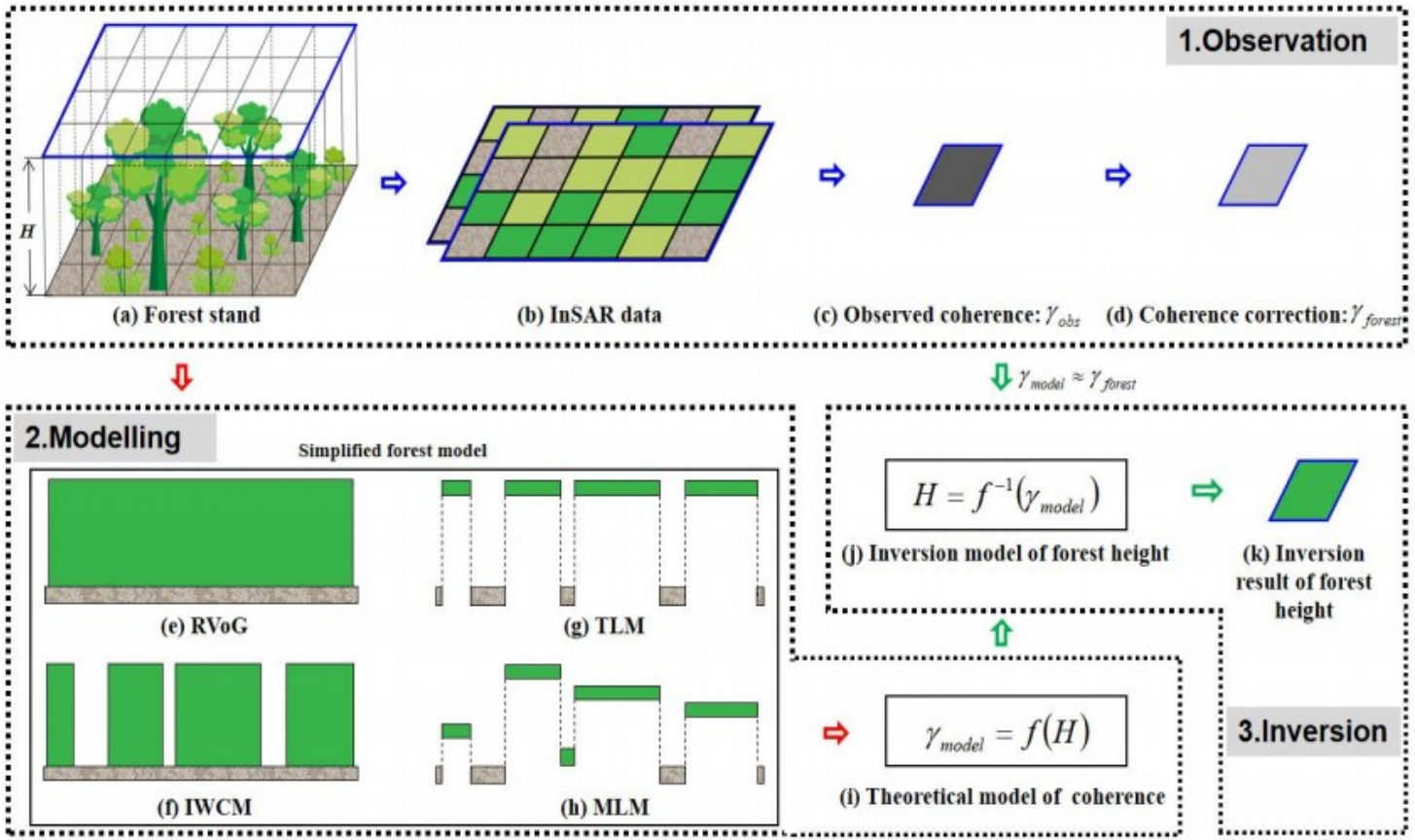

(1)Coherence calculation

(2) InSAR coherence model

Zhao Lei,et al. A new approach for forest height inversion using X-band single-pass InSAR coherence data [J]. *IEEE Transactions on Geo. RS*, 2021, doi: 10.1109/TGRS. 2021.3072125.

(1) Coherence calculation method from InSAR data

Coherence	Calculation equations
$\gamma_{def.int}$	$\left\|\sum_{i=1}^{N}\sqrt{a_{1,i}a_{2,i}}\cdot e^{j\Phi_i}\right\| \Big/ \sqrt{\sum_{i=1}^{N}a_{1,i}\cdot\sum_{i=1}^{N}a_{2,i}}$
$\gamma_{def.flt}$	$\left\|\sum_{i=1}^{N}\sqrt{a_{1,i}a_{2,i}}\cdot e^{j\Phi_i}\cdot e^{-j\Phi_{flt,i}}\right\| \Big/ \sqrt{\sum_{i=1}^{N}a_{1,i}\cdot\sum_{i=1}^{N}a_{2,i}}$
$\gamma_{def.top}$	$\left\|\sum_{i=1}^{N}\sqrt{a_{1,i}a_{2,i}}\cdot e^{j\Phi_i}\cdot e^{-j\Phi_{flt,i}}\cdot e^{-j\Phi_{top,i}}\right\| \Big/ \sqrt{\sum_{i=1}^{N}a_{1,i}\cdot\sum_{i=1}^{N}a_{2,i}}$
$\gamma_{pha.int}$	$\left\|\sum_{i=1}^{N}e^{j\Phi_i}\right\|$
$\gamma_{pha.flt}$	$\left\|\sum_{i=1}^{N}e^{j\Phi_i}\cdot e^{-j\Phi_{flt,i}}\right\|$
$\gamma_{pha.top}$	$\left\|\sum_{i=1}^{N}e^{j\Phi_i}\cdot e^{-j\Phi_{flt,i}}\cdot e^{-j\Phi_{top,i}}\right\|$

Traditional method

The assumption for the coherence modeling is not considered

Phase based

Proposed method

(2) InSAR coherence modeling for forest vegetation

The penetration of short wavelength SAR into forest is mainly gap penetration rather than medium penetration

Coherence estimation with ML method:

$$\gamma_{Obs}=\frac{\left|\sum_{i=1}^{N}\sqrt{a_{1,i}a_{2,i}}\cdot e^{j\Phi_i}\right|}{\sqrt{\sum_{i=1}^{N}a_{1,i}\cdot\sum_{i=1}^{N}a_{2,i}}}$$

Assuming：

- Master and slave *BSC* have no difference
- InSAR phase after plat and topo removal ；
- *BSC* don't change in the same height ；

MLM:

$$\gamma_{MLM}=\frac{\left|\int_0^H f(h)\sigma(h)e^{jk_z h}dh\right|}{\int_0^H f(h)\sigma(h)dh}$$

- *BSC* don't change in vertical direction ；

Simplified MLM:

$$\gamma_{Model\_MLM}=\left|\int_0^H f(h)e^{jk_z h}dh\right|$$

Assuming *f(h)* is of different distribution.

- Two-Point Distribution → TLMm
- Uniform Distribution → SINC
- Mixed Truncated Normal Distribution → MTND

A new approach for forest height inversion using X-band single-pass InSAR coherence

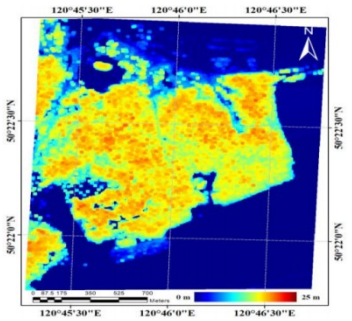

LiDAR H100

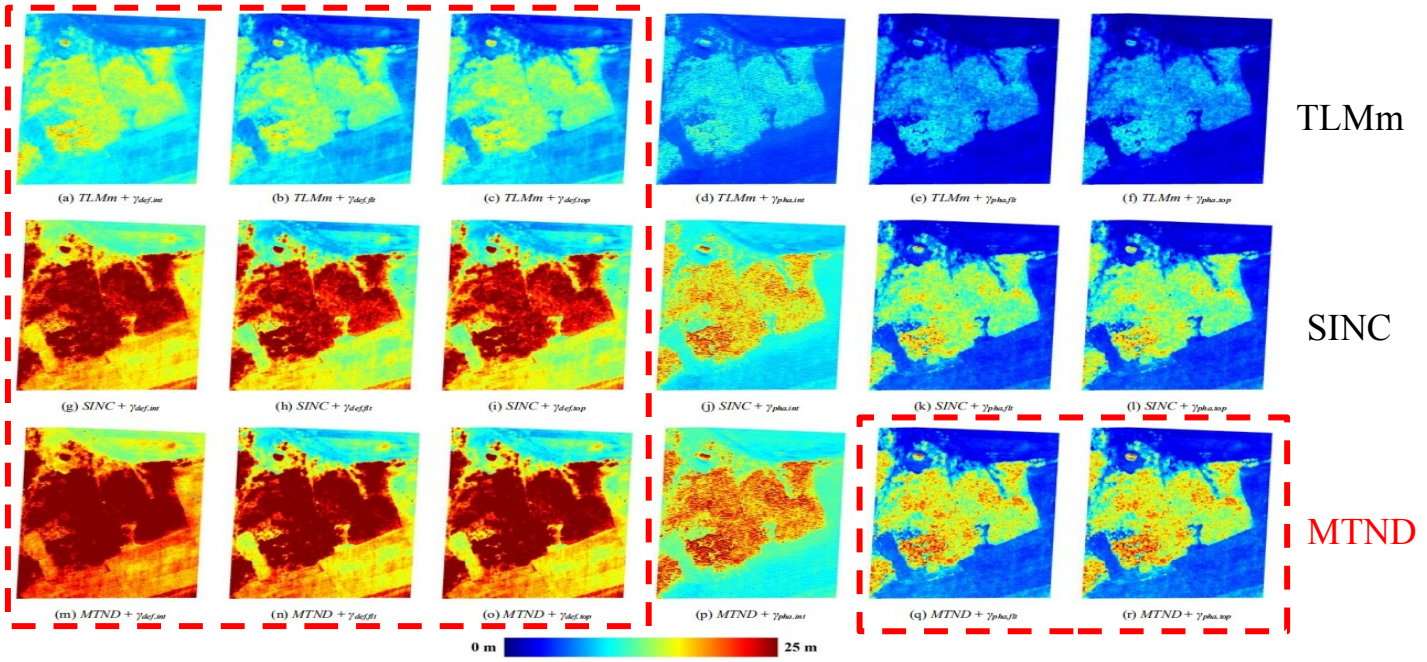

TLMm

SINC

MTND

TLMm model under estimation forest height， take $\gamma_{pha.flt}$/$\gamma_{pha.top}$ as inputs MTND model is of highest accuracy

Forest height estimation from X- and P-band InSAR data

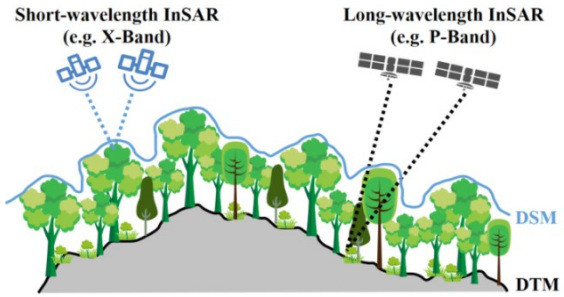

Under-estimate DSM Over-estimate DTM

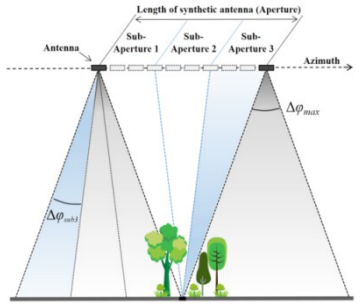

Sub-aperture decomposition to get the true ground surface phase

(Fu, H. et al, remote sensing,2017)

Acc.=86.6%
RMSE=1.8m

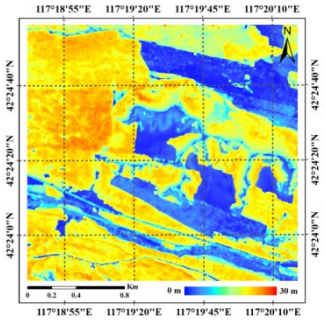

LiDAR H100

validation

DSM bias MLM

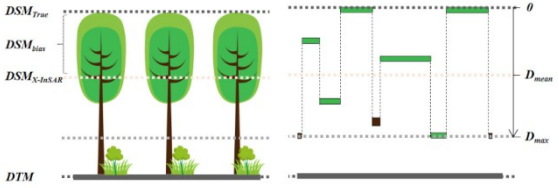

$$f(x) = \frac{1}{D_{max}}, x \in (0, D_{max})$$

$$DSM_{\text{bias}} = \text{Dmax}/2 = \frac{\pi}{|k_z|}\left(1 - \frac{2}{\pi}\sin^{-1}\left[|\gamma|^{0.8}\right]\right)$$

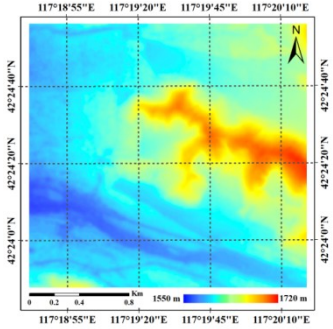

DSM after bias compensation

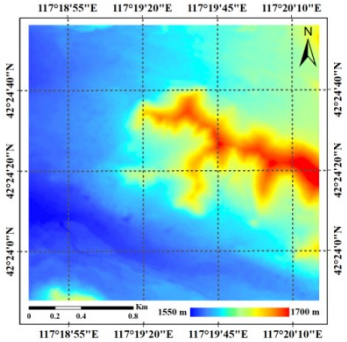

DTM derived from sub-aperture

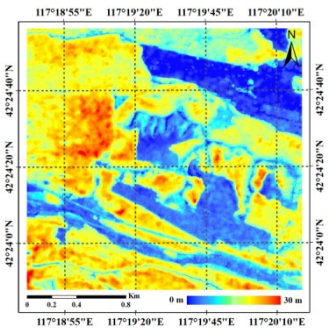

Forest height

(Xu K., Zhao L., et al, remote sensing,2022)

TomoSAR—Forest underlying topography estimation

Dual polarimetric TomoSAR (DP-TomoSAR) is proposed as a suitable candidate to estimate forest underlying topography because of its wide swath and multiple polarimetric observations.

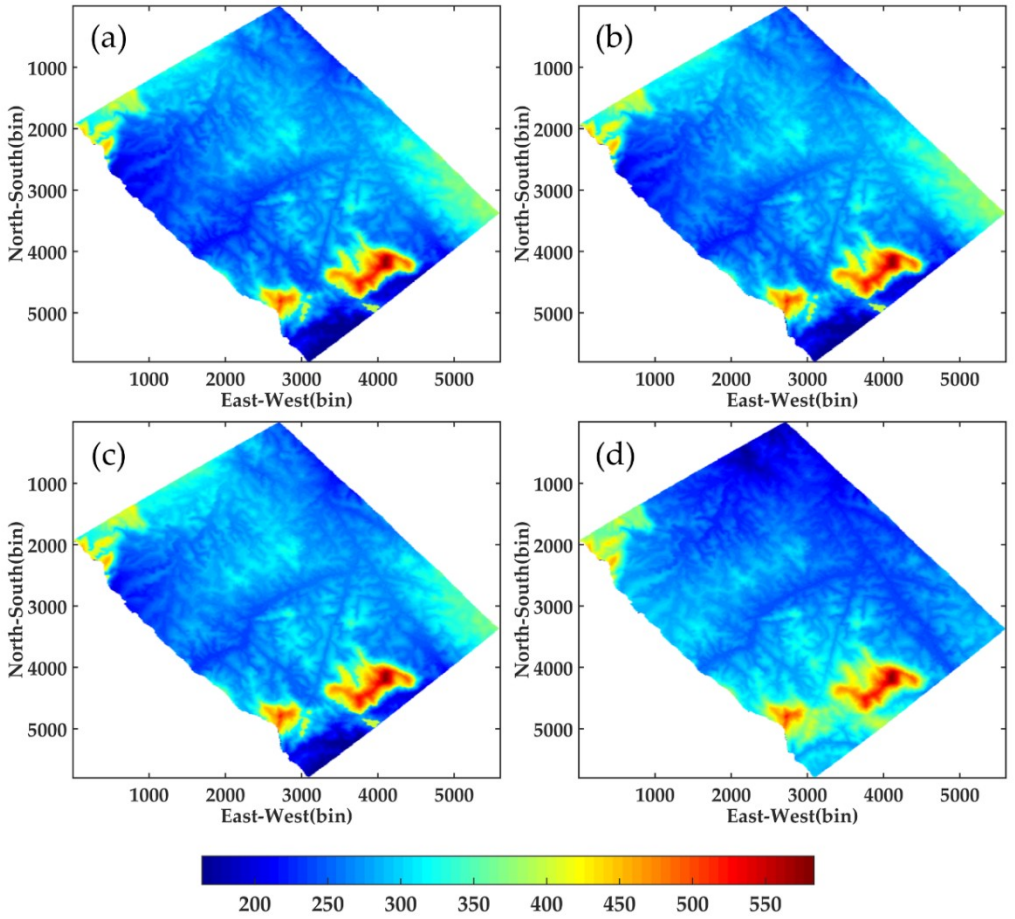

Underlying topography: (a) DP-Beamforming (b) DP-Capon (c) DP-MUSIC and (d) LiDAR

Table 1. RMSE of underlying topography estimated by different algorithms using SP-TomoSAR, DP-TomoSAR and FP-TomoSAR.

Method	Data Type	RMSE (m)
Beamforming	SP	9.24
	DP	8.25
	FP	8.07
Capon	SP	9.20
	DP	8.09
	FP	7.92
MUSIC	SP	9.18
	DP	8.17
	FP	8.01

The underlying topography obtained by different DP-TomoSAR algorithms maintain a high consistency in texture features. The accuracy of the results retrieved by all the three algorithms using DP-TomoSAR and FP-TomoSAR is close, and both of them are superior to those of SP-TomoSAR.

Xing Peng, Youjun Wang, Shilin Long, Xiong Pan, Jianjun Zhu, Xinwu Li. Underlying Topography Inversion Using TomoSAR Based on Non-Local Means for an L-Band Airborne Dataset. Remote Sensing, 2021, 13(15), 2926.

CAS, AIRCAS, RADI, X,. Li

TomoSAR—Forest underlying topography estimation

Nonlocal means(NLM) TomoSAR on ESA BioSAR 2008 datasets

	Beamforming	Capon	MUSIC
LM	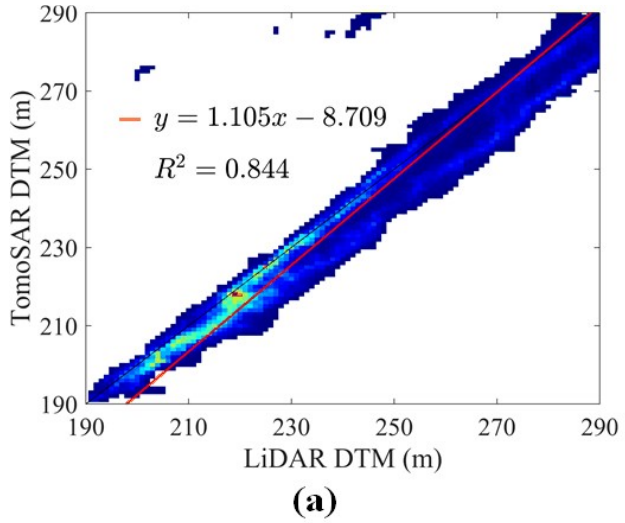	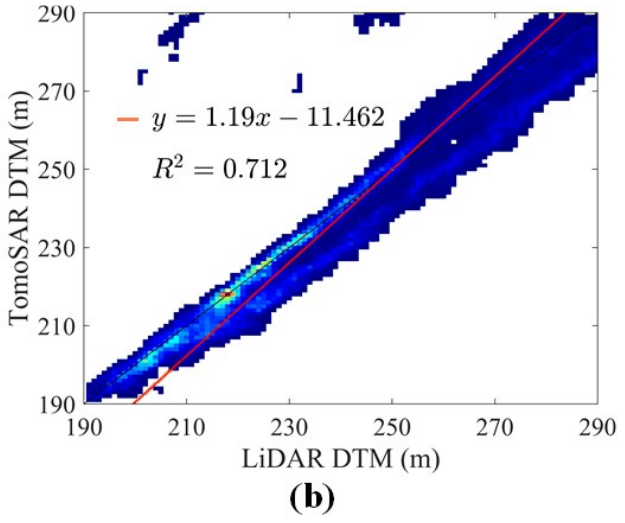	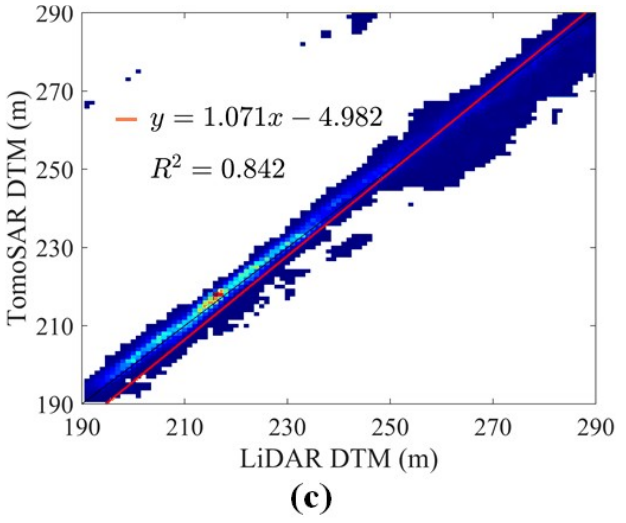
	(a) $y = 1.105x - 8.709$, $R^2 = 0.844$	(b) $y = 1.19x - 11.462$, $R^2 = 0.712$	(c) $y = 1.071x - 4.982$, $R^2 = 0.842$
NLM	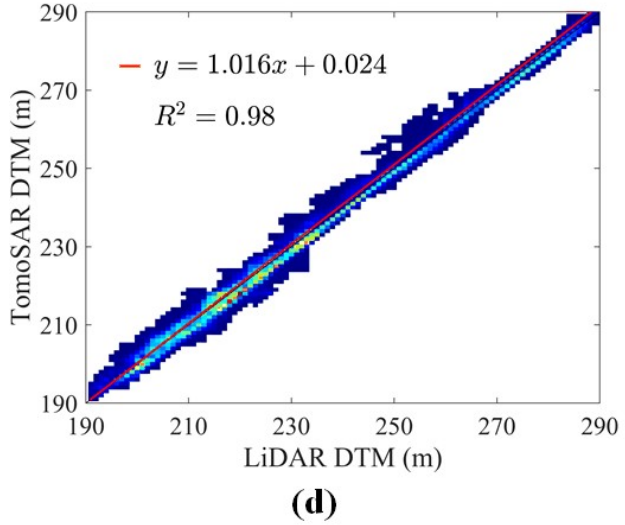	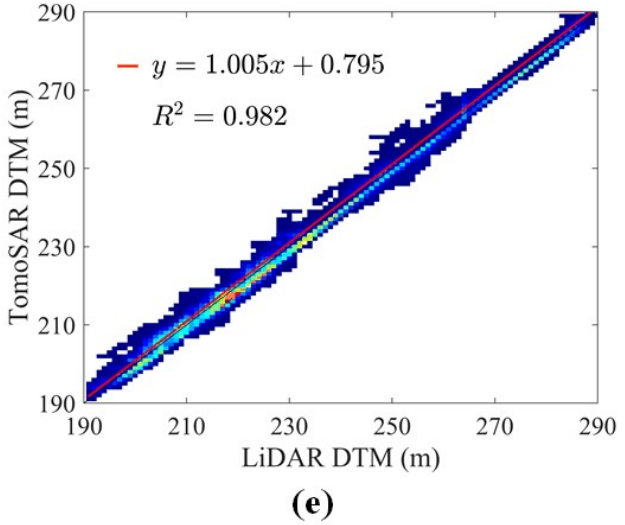	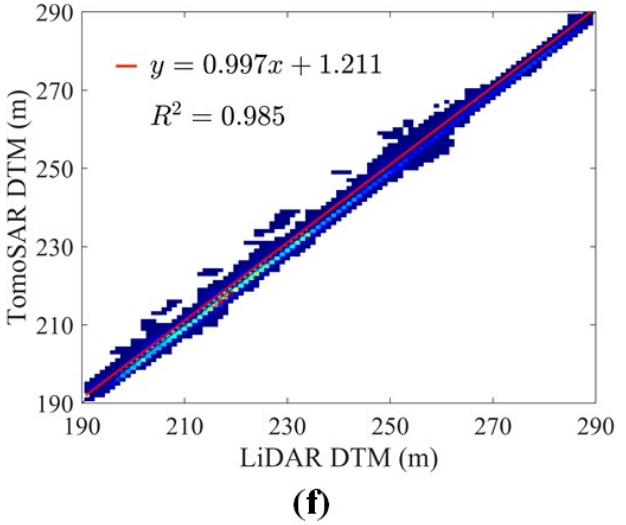
	(d) $y = 1.016x + 0.024$, $R^2 = 0.98$	(e) $y = 1.005x + 0.795$, $R^2 = 0.982$	(f) $y = 0.997x + 1.211$, $R^2 = 0.985$

TomoSAR——Building height estimation

TomoSAR reconstruction algorithm based on **CS atomic norm minimization (Tomo-ANM)**. ANM is a continuous compressed sensing technique, and its fast realization, IVDST, is utilized to accelerate the process. SL1MMER is shown as a reference.

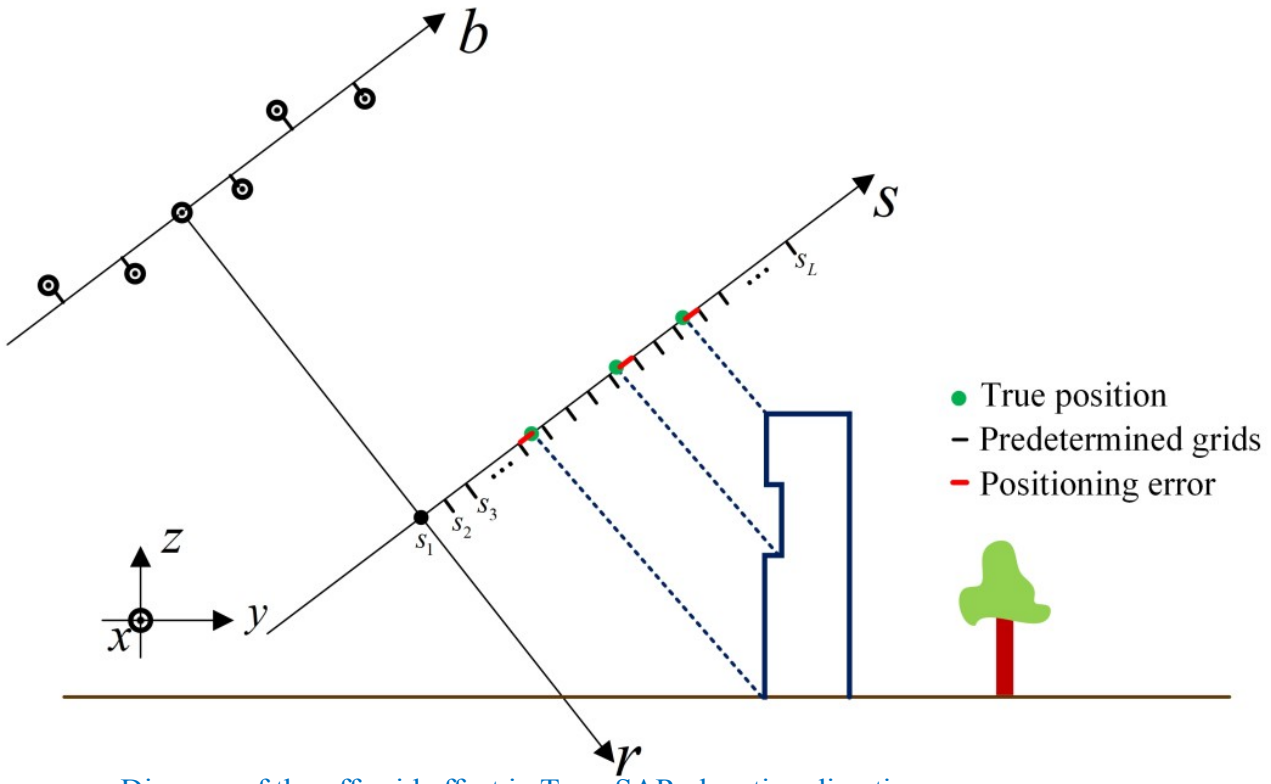

Diagram of the off-grid effect in TomoSAR elevation direction.

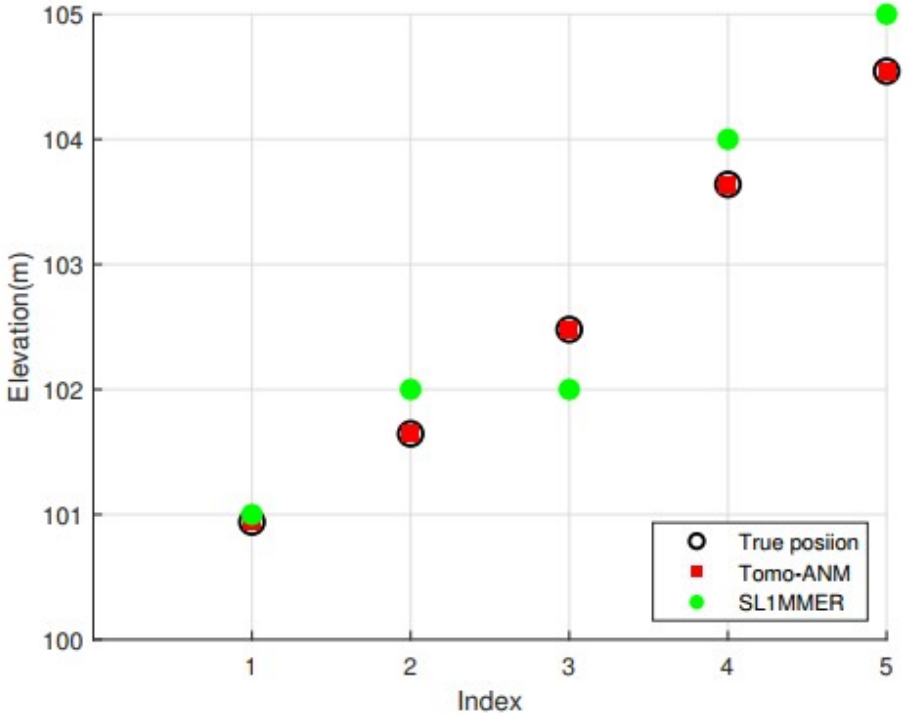

Removal of the off-grid effect by Tomo-ANM.

TomoSAR——Building height estimation

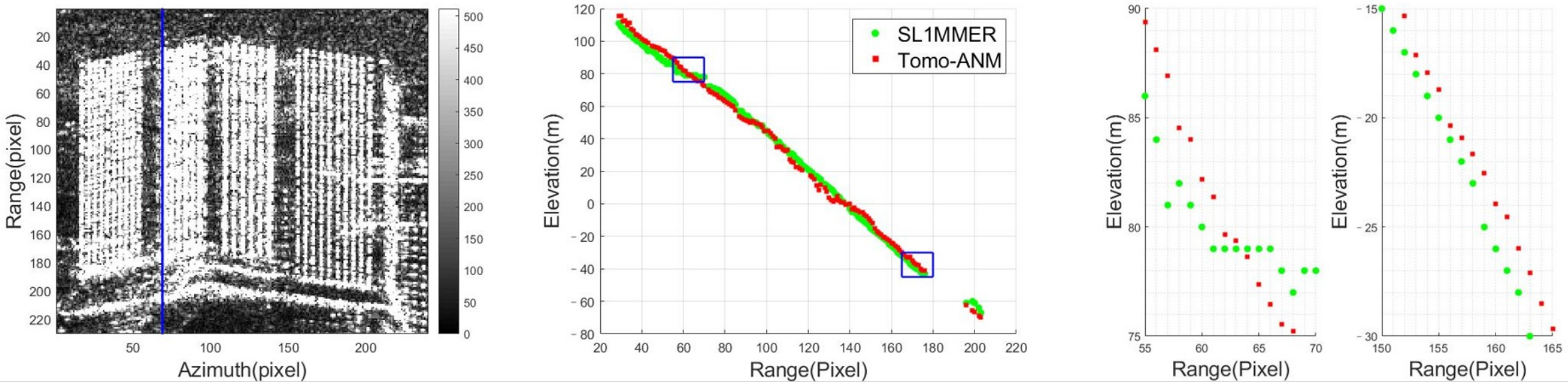

Real data results: (a) SAR image. Blue line is used to show tomographic profiles . (b) The Tomo-ANM and SL1MMER profiles of line azimuth 69. (c) Partial enlargement of the blue rectangle in (b).

Table 1. Height estimation of different methods. The true height of the building is 99 m.

	Building Height(m)	Estimation Error(m)
Tomo-ANM-CVX	**96.62**	2.40%
Tomo-ANM-IVDST	**95.70**	3.33%
SL1MMER	91.84	7.23%

We used eight stacks TerraSAR staring spotlight data to conduct real data experiments. The results showed that, compared with the on-grid algorithm, Tomo-ANM can eliminate the off-grid effect, so as to better position scatterers and obtain more accurate building height estimation results.

Ning Liu, Xinwu Li, Xing Peng, Wen Hong, SAR Tomography Based on Atomic Norm Minimization in Urban Areas. *Remote Sensing.* **2022**, *14*,

Côté Ouest de la tour

Réseau des 20 antennes bandes P+L

6 antennes bande C

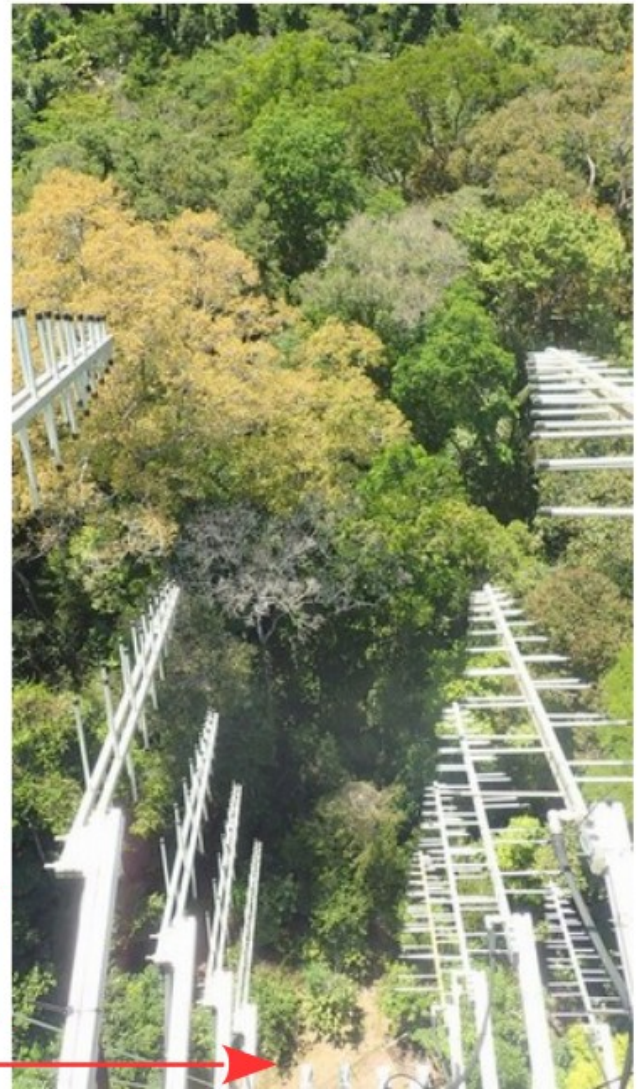

Côté Nord-Est de la tour

2 antennes large bande (6-18GHz)

6 antennes bande C

Tropiscatm Paracou, French Guyana

Preparation of ESA's BIOMASS mission
Insights of TowerScat campaigns

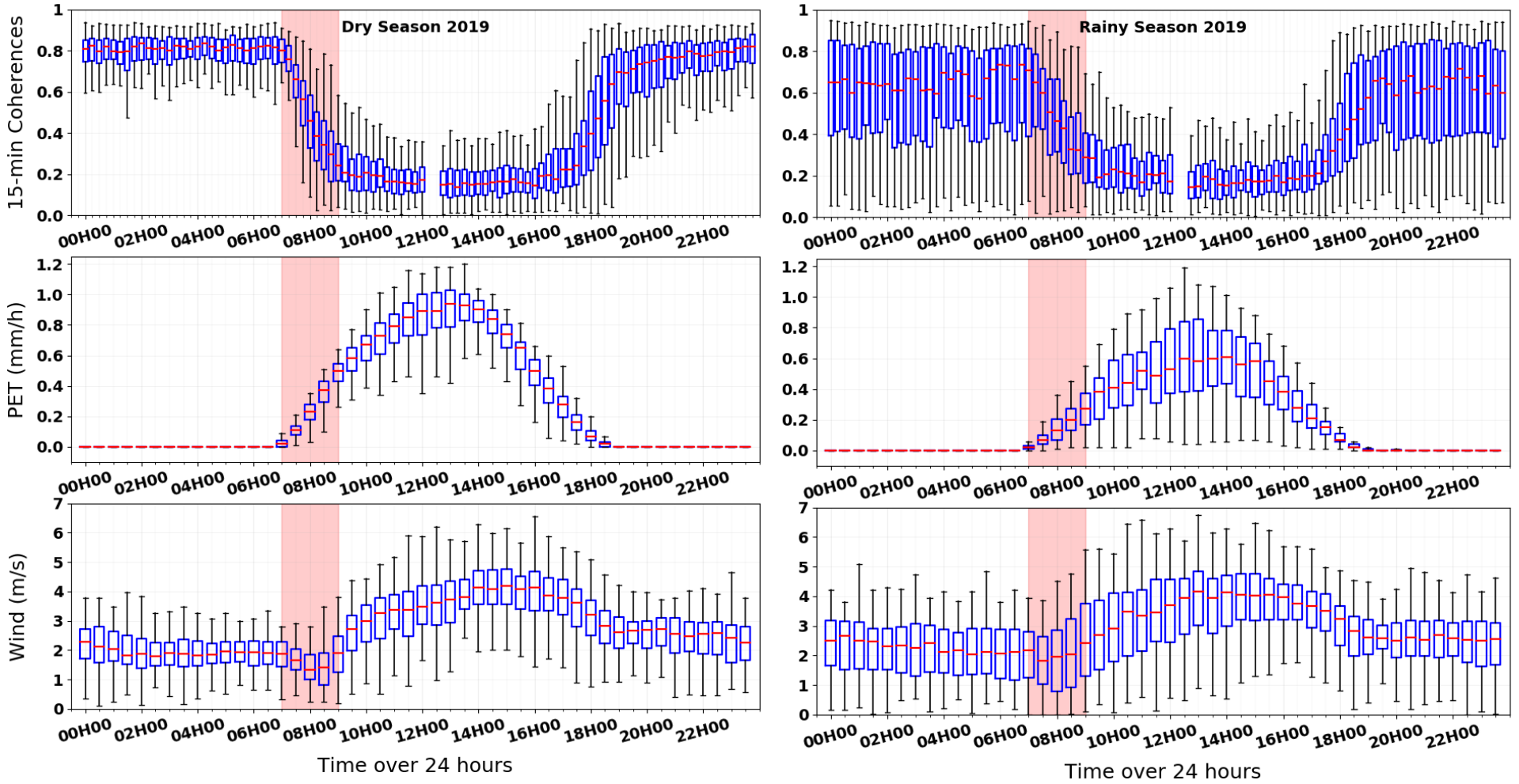

C-band 15mn-decorrelation patterns can be explained by evapotranspiration, not wind speed

El Idrissi Essebtey, Villard 2021, 2022

Preparation of ESA's BIOMASS mission Insights of TowerScat campaigns

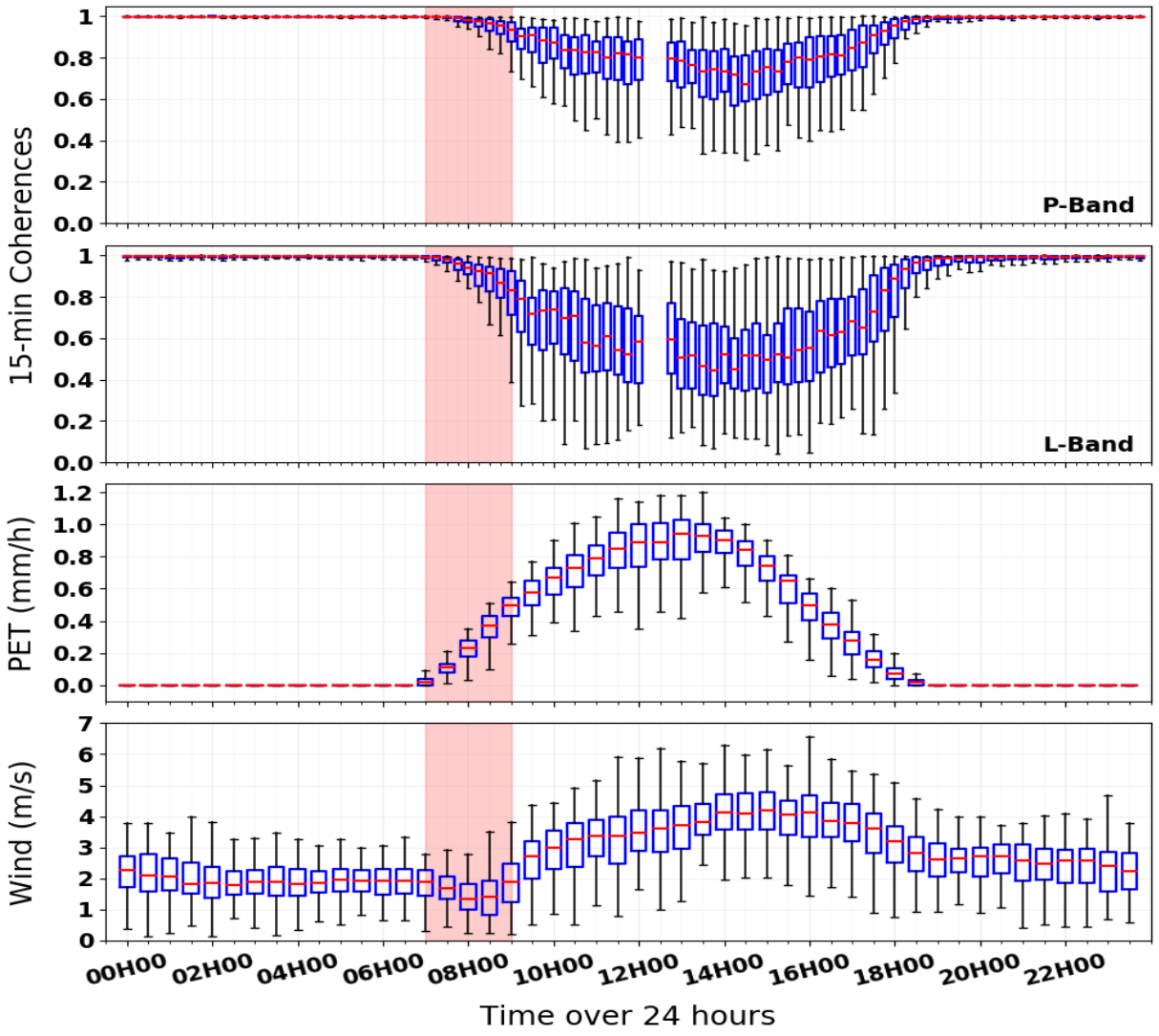

Evapotranspiration plays a key role at L an P bands too

Preparation of ESA's BIOMASS mission
Forest characterization using signal processing techniques

Ground and tree height estimation
- geophysical relevance
- comparizon/complementarity with other EO missions

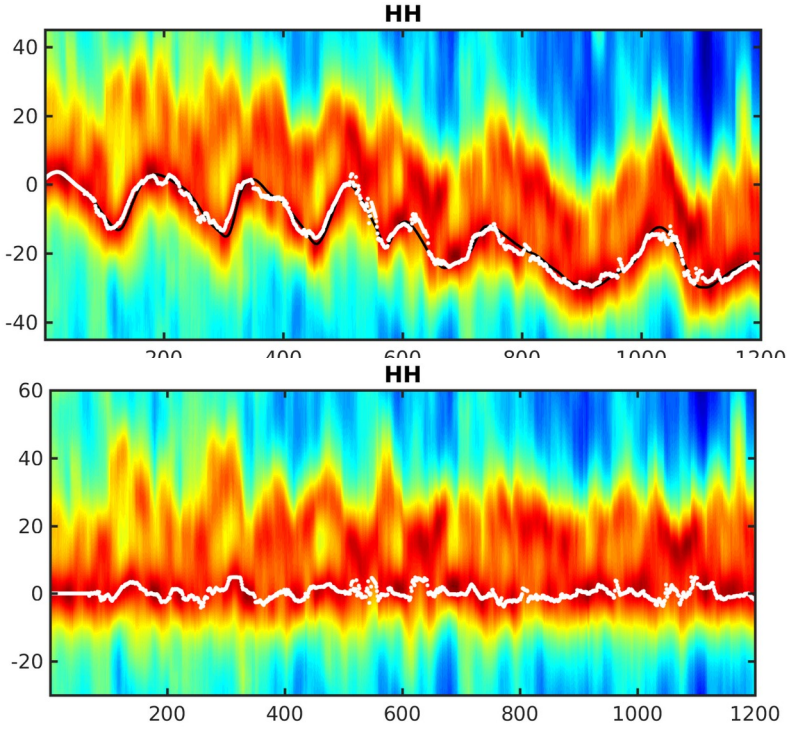

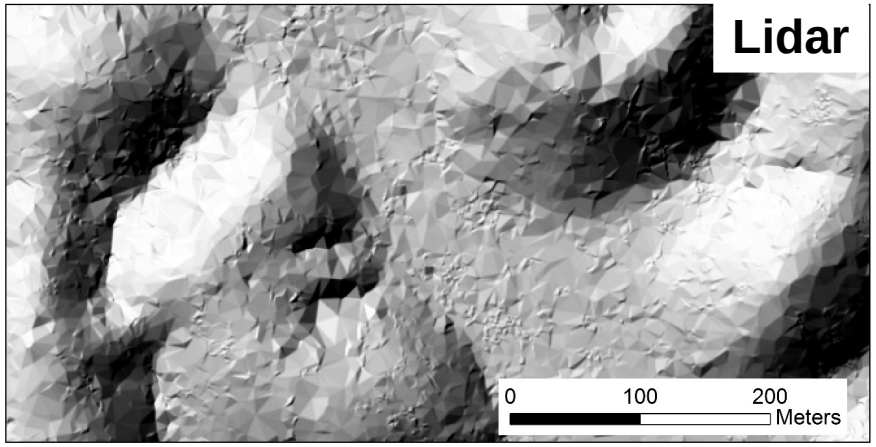

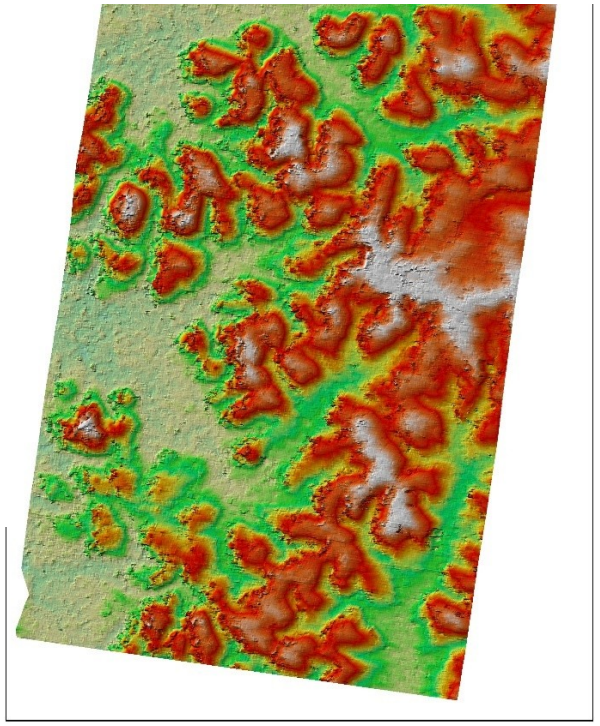

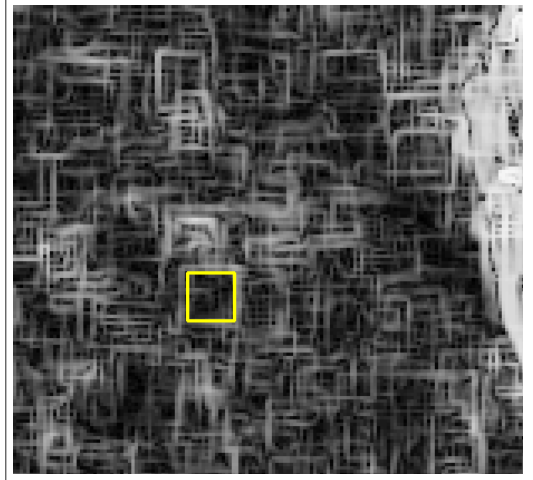

Preparation of ESA's BIOMASS mission
Forest characterization using signal processing techniques

Ground and tree height estimation
- geophysical relevance
- comparizon/complementarity with other EO missions

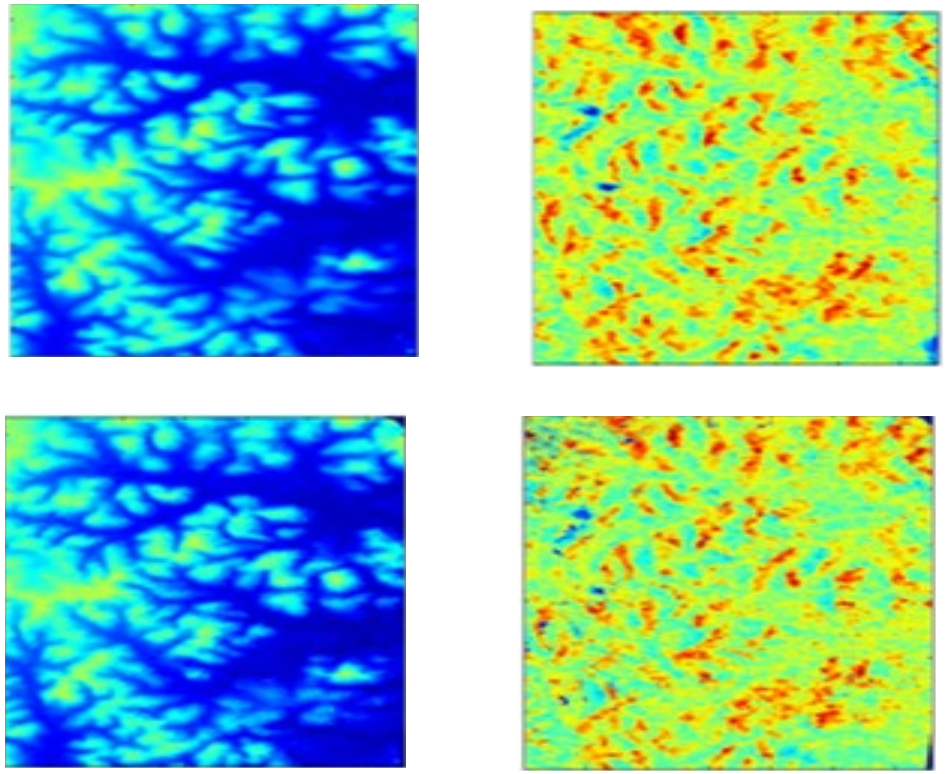

P-band TomoSAR

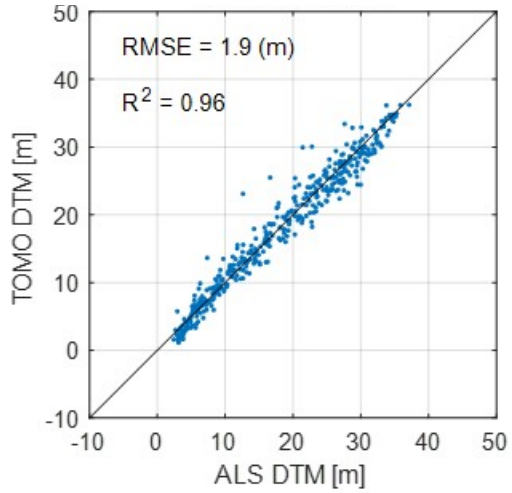

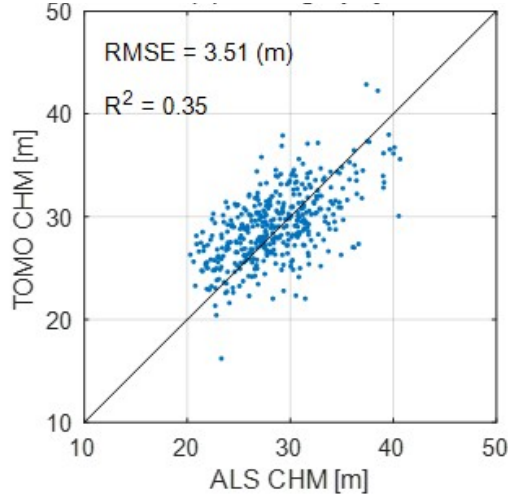

GEDI

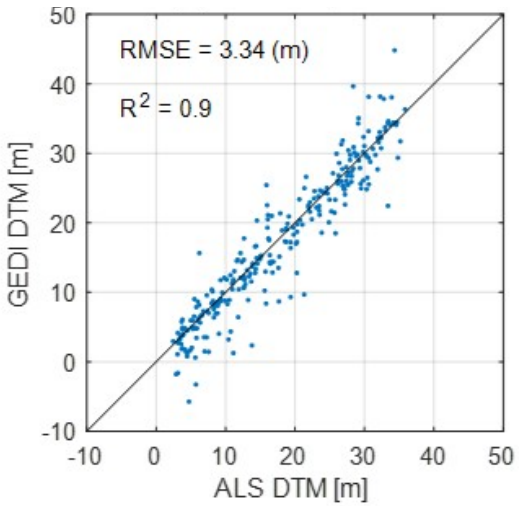

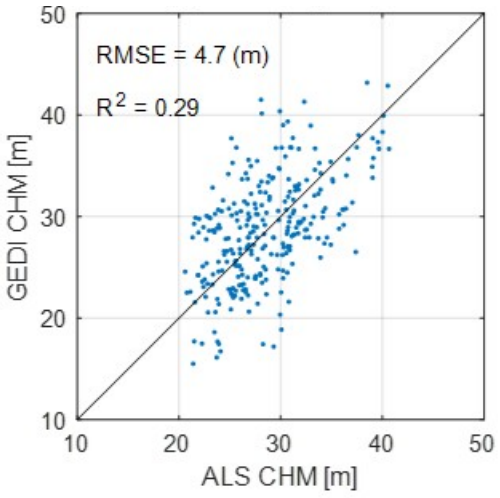

Adaptive HR retrieval of a tropical forest structure at P band

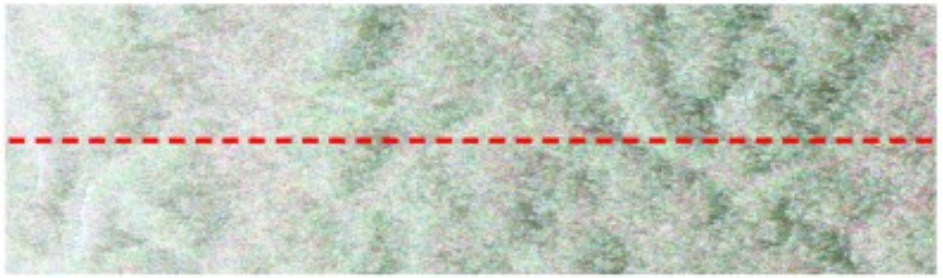

(a) Test line

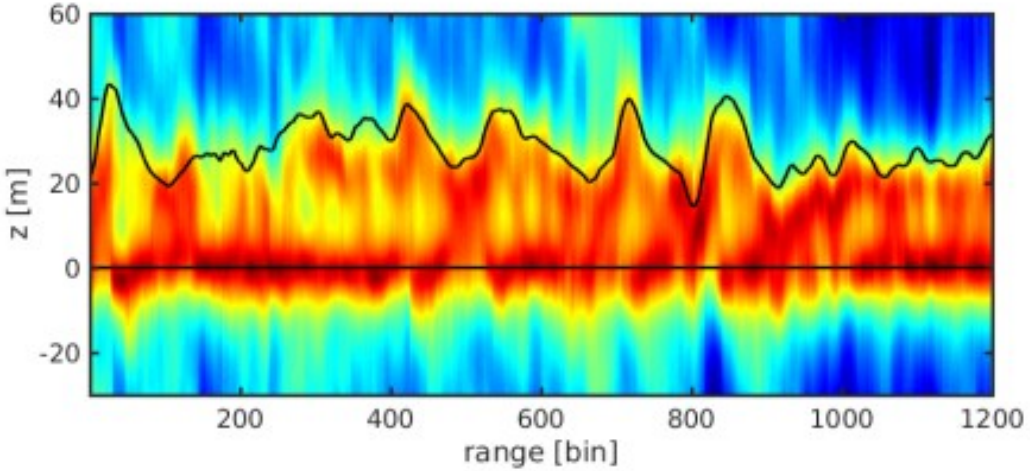

(b) Capon tomogram using $\widehat{\mathbf{R}}$

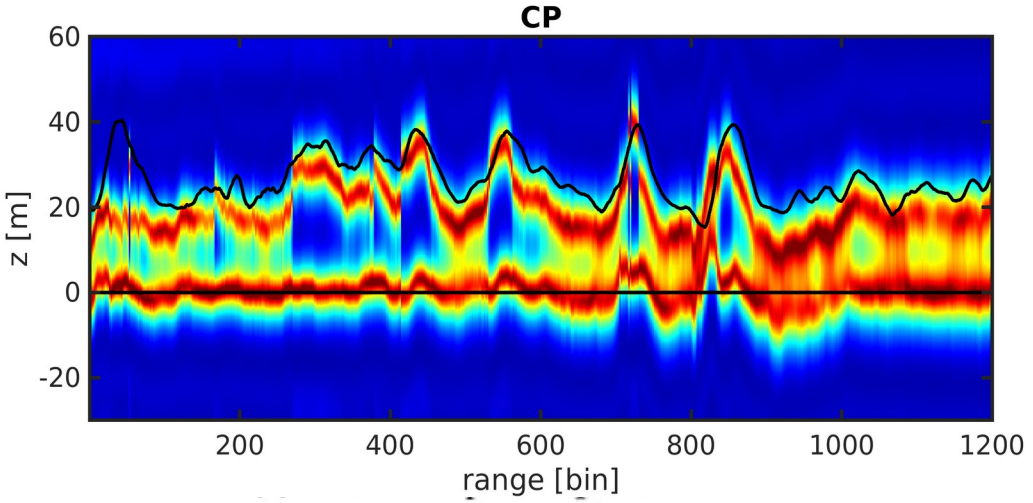

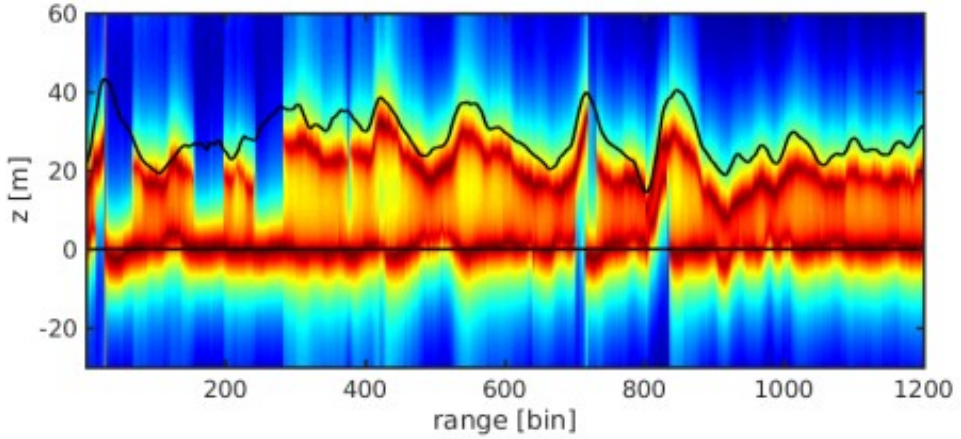

(d) Capon tomogram using $\mathbf{R}(\widehat{\alpha})$

Preparation of ESA's BIOMASS mission
BIOMASS programmatic sequence

BIOMASS mission sequence of operating modes

Tomographic Phase:
7 x 3-day repeat
15 months for global coverage

Interferometric Phase:
3 x 3-day repeat; 7 months for global coverage
≈ 4 years time series

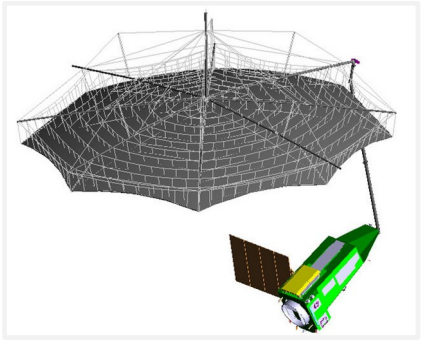

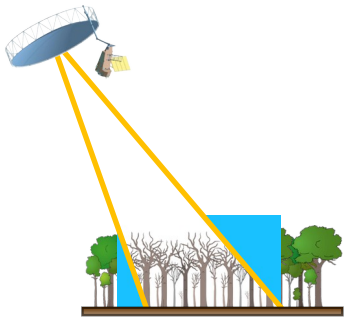

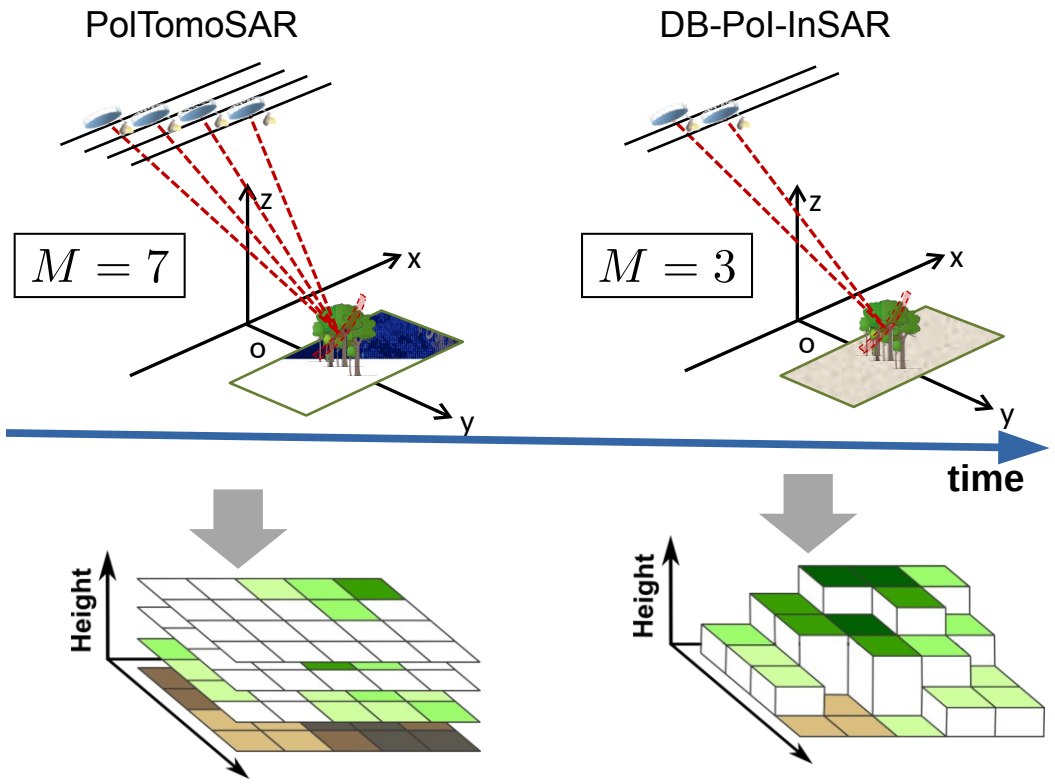

→ **Synergistic use of priors**

→ **Performance quantification**

Standard deviation of tree height estimates

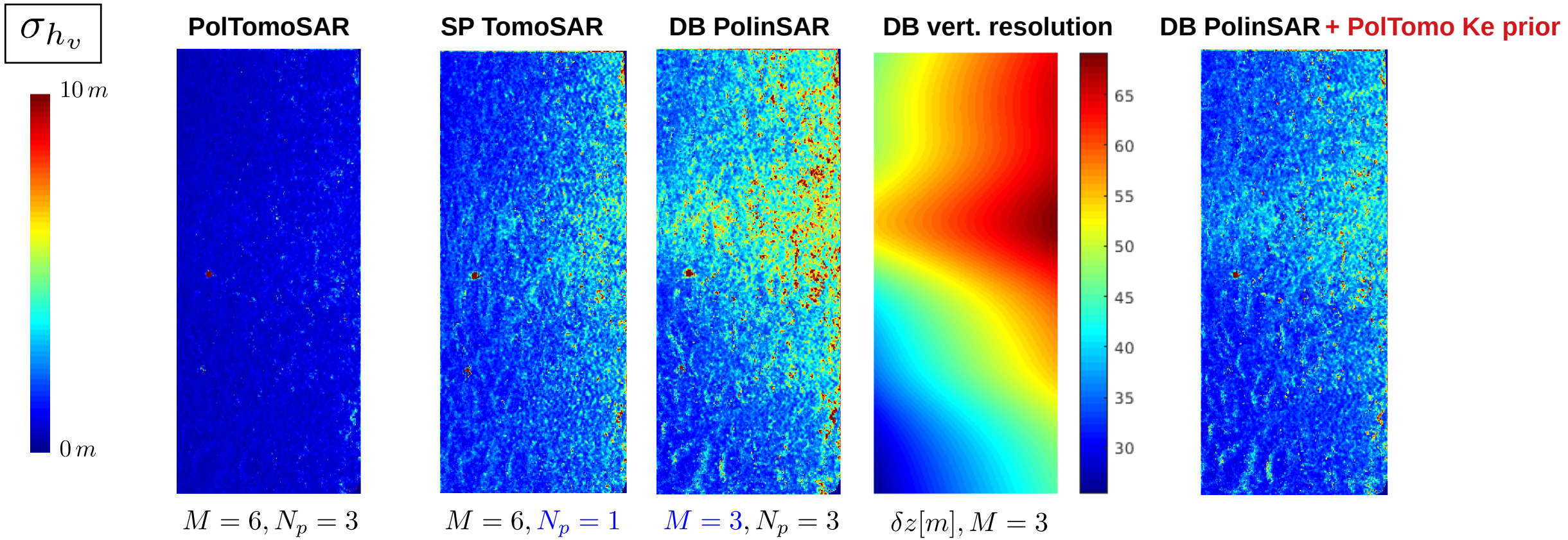

- **Absolute variability values depend on processing configuration**
- **Sensitivity to vertical resolution**
- **Auxiliary information (priors) → overcome resolution related issues**

Near-Real Time deforestation monitoring using S1

- 12 days (6 in Europe) time-series → NRT capabilities
- C-band: forest loss detection affected by
  - changing environmental factors (soil moisture...)
  - residual (or regrowing) vegetation

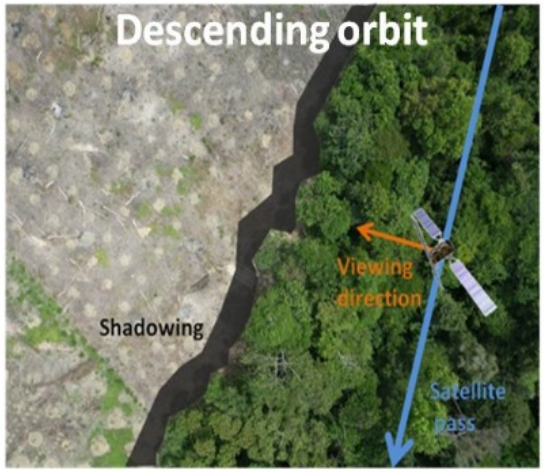

10 May 2015

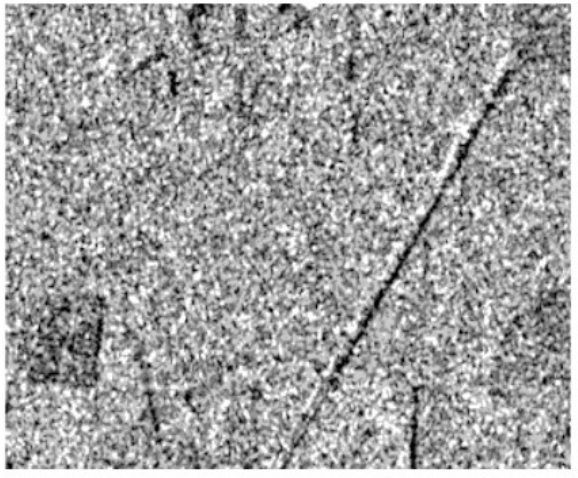

1 October 2016

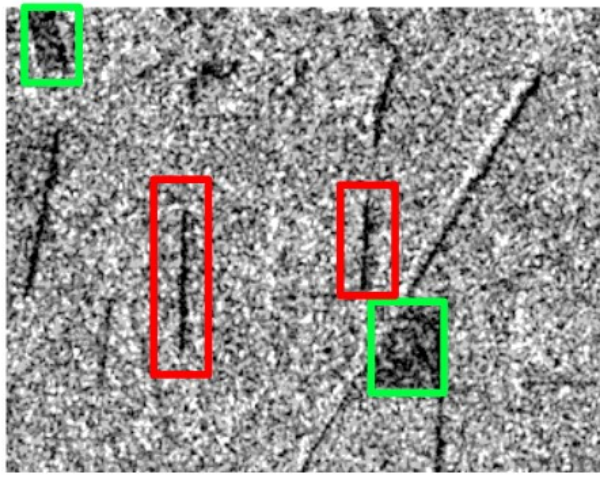

Recent logging
Older logging shadow edge

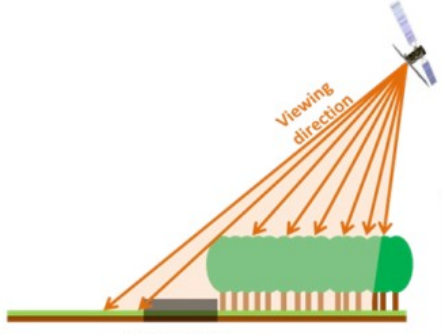

10 m resolution,
>90% accuracy (Peru, Gabon, French Guiana, Brasil and Vietnam)

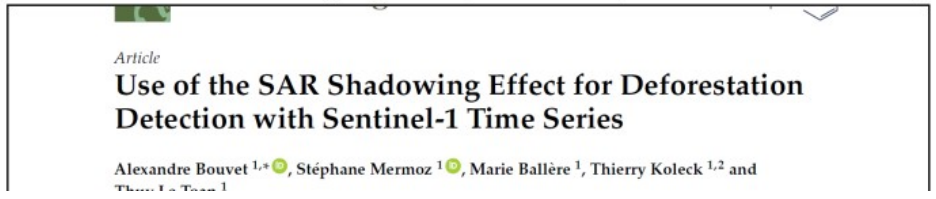

Article

Use of the SAR Shadowing Effect for Deforestation Detection with Sentinel-1 Time Series

Alexandre Bouvet [1,*], Stéphane Mermoz [1], Marie Ballère [1], Thierry Koleck [1,2] and

Monitoring forest disturbance in French Guyana

https://www.spaceclimateobservatory.org/tropisco-amazonia

Remote Sensing of Environment
Volume 252, January 2021, 112159

SAR data for tropical forest disturbance alerts in French Guiana: Benefit over optical imagery

Marie Ballère [a, b, c], Alexandre Bouvet [d], Stéphane Mermoz [d, e], Thuy Le Toan [d], Thierry Koleck [a], Caroline Bedeau [f], Mathilde André [f], Elodie Forestier [f], Pierre-Louis Frison [c], Cédric Lardeux [g]

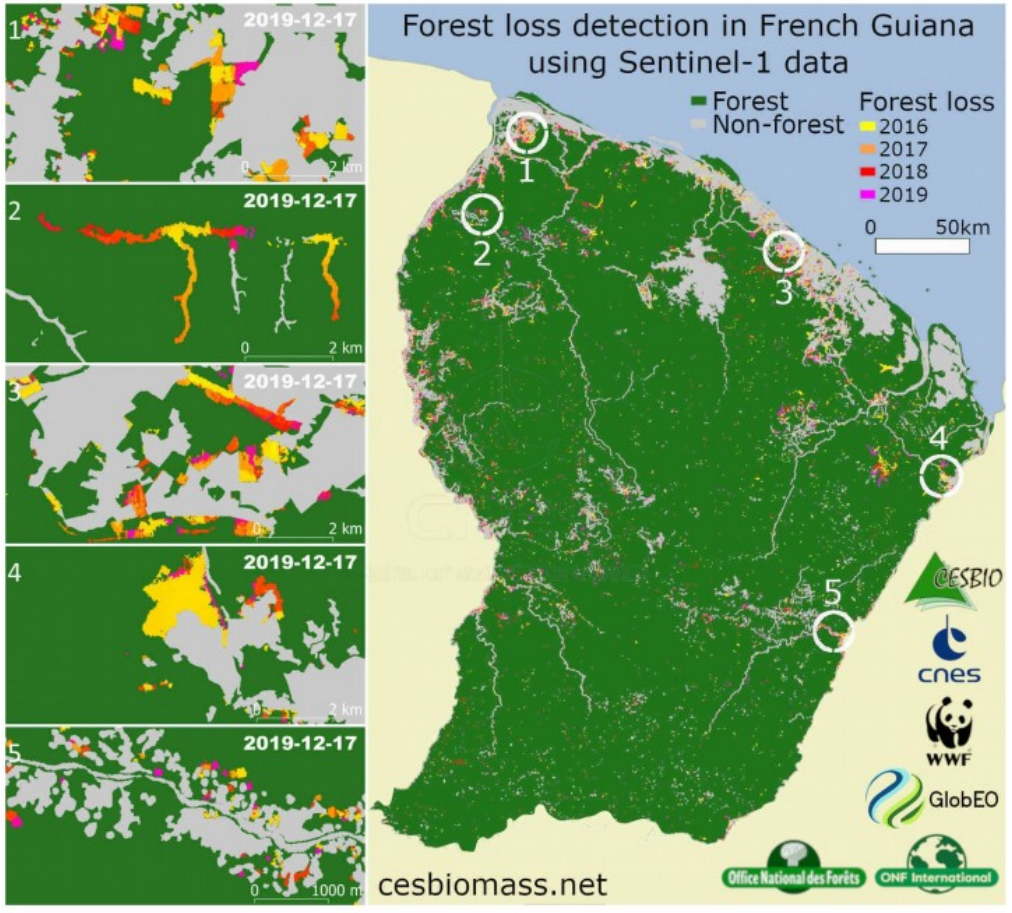

Drivers: gold mining, smallholder agriculture and forest exploitation

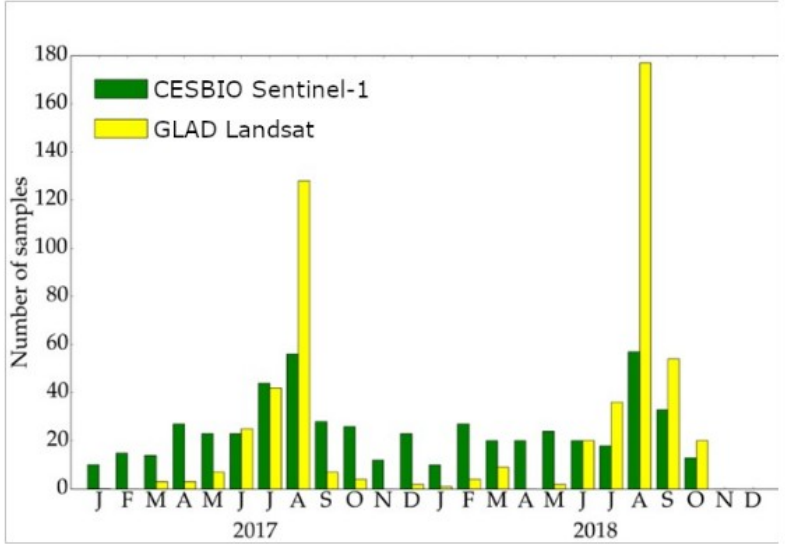

Validated using **1 867 in situ plots** covering 2 124.5 ha: **UA of 96.2%** and **PA of 81.5%**

Monitoring forest disturbance in tropical regions

https://www.spaceclimateobservatory.org/tropisco-amazonia

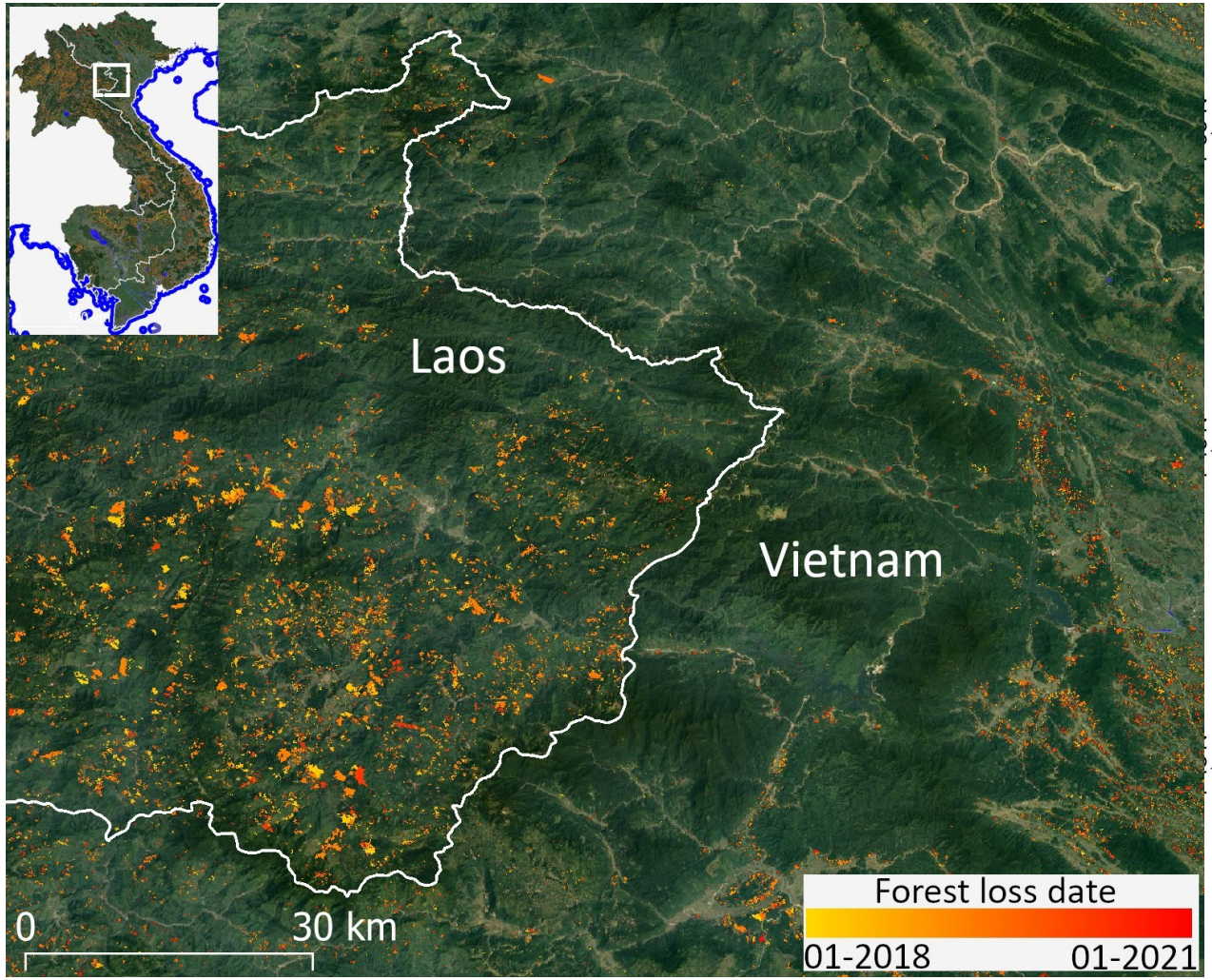

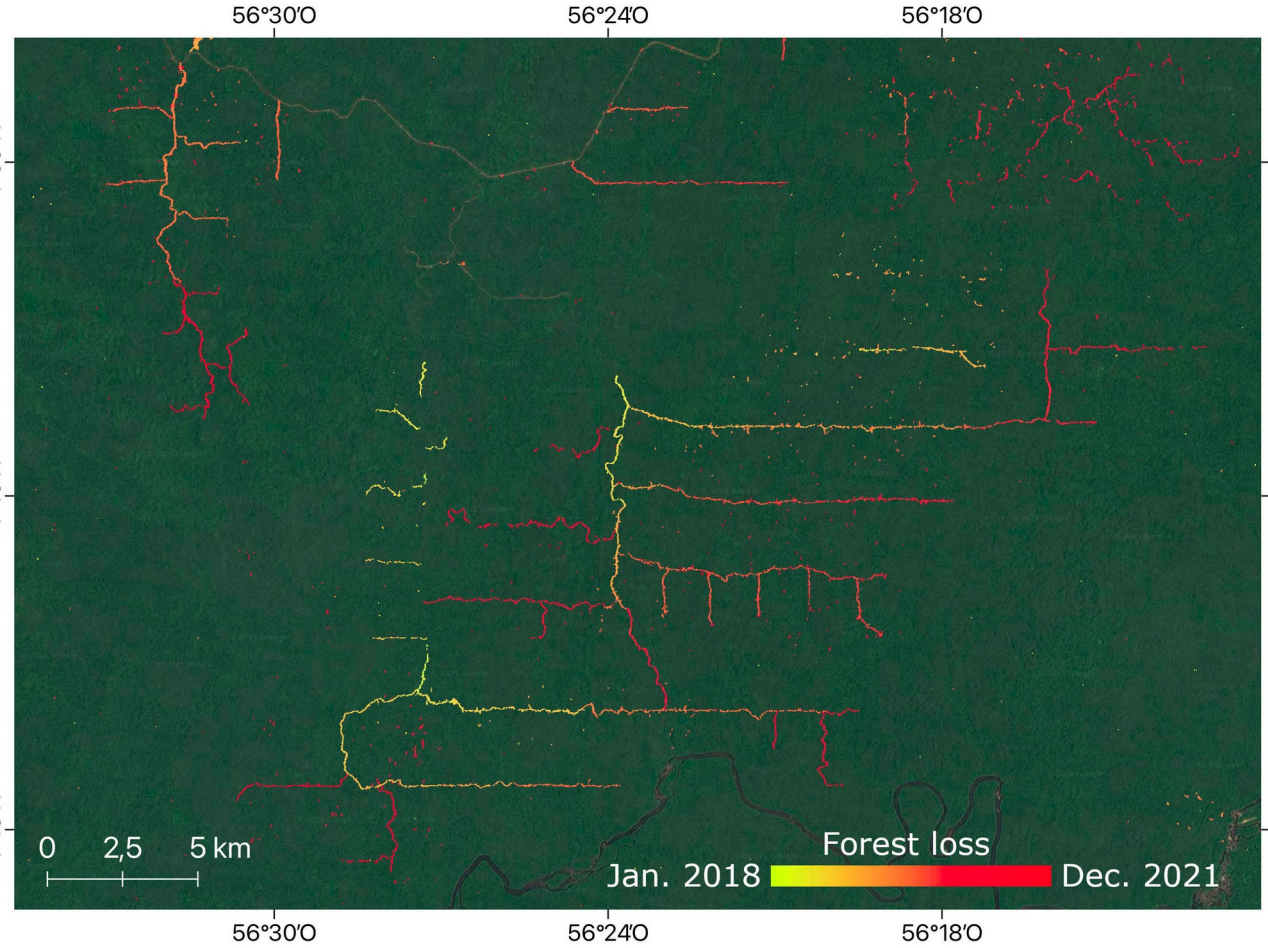

PolSARpro and community events

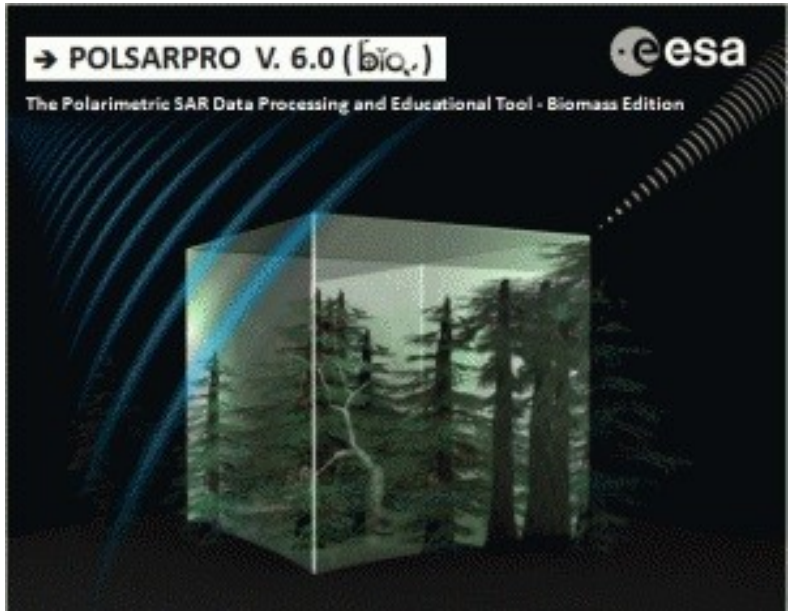

U. Rennes 1, IETR, E. Pottier

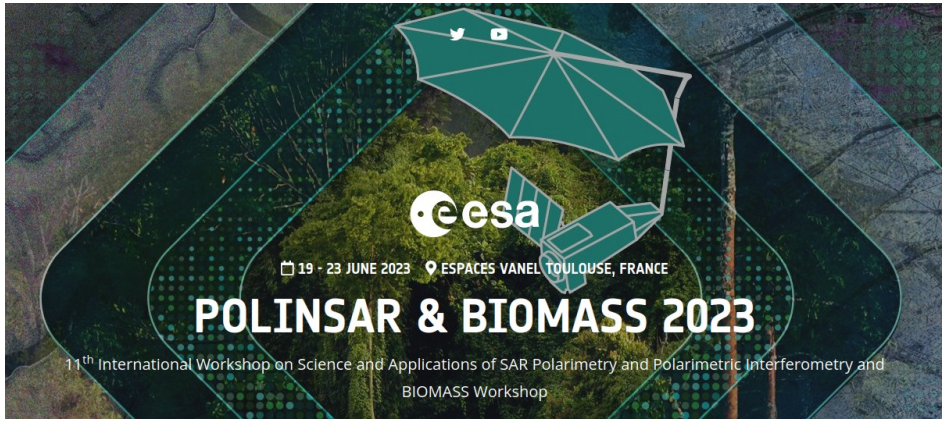

- **ESA PolinSAR & BIOMASS workshop**

  Toulouse, France, 19-23 june 2023

- **ESA SAR polarimetry training**

  Toulouse, France, 12-16 june 2023

- Qiang Yin, Junlang Li, Yongsheng Zhou, Deliang Xiang & Fan Zhang. Adaptive weighted learning for vegetation contribution in soil moisture inversion using PolSAR data, International Journal of Remote Sensing, 2022, 43:9, 3190-3215.
- Qiang Yin; Jie Xu; Deliang Xiang*; et al. Polarimetric Decomposition With an Urban Area Descriptor for Compact Polarimetric SAR Data. IEEE Journal of Selected Topics in Applied Earth Observations and Remote Sensing, 2021, 14: 10033-10044.
- Qiang Yin; Junlang Li; Fei Ma*; et al. Dual-Channel Convolutional Neural Network for Bare Surface Soil Moisture Inversion Based on Polarimetric Scattering Models. Remote Sensing, 2021, 13(22): 4503.
- Ying Luo； Qiang Yin*； Fei Ma； A Discrimination Method of Water and Shadow Areas Based on Polarization Entropy of Sentinel-1 Data， IEEE International Geoscience and Remote Sensing Symposium (IGARSS), 2022.07.17-22.
- Shasa Deng; QiangYin*; Fan Zhang; Xinzhe Yuan; A Ship Ghost Interference Removal Method Based on GaoFen-3 Polarimetric SAR Data, IEEE International Geoscience and Remote Sensing Symposium (IGARSS), 2022.07.17-22.
- Zhiyuan Lin; Qiang Yin*； Yongsheng Zhou； Jun Ni； Fei Ma; Time-series PolSAR Crop Classification Based on Joint Feature Extraction, IEEE International Geoscience and Remote Sensing Symposium (IGARSS), 2022.07.17-22.
- Zhao Lei, Chen Erxue, Li Zengyuan, et al. A New Approach for Forest Height Inversion Using X-Band Single-Pass InSAR Coherence Data. IEEE Transactions on Geoscience and Remote Sensing, 2022, 60: 5206018. DOI:10.1109/TGRS.2021.3072125
- Xu, K.; Zhao, L.; Chen, E.; Li, K.; Liu, D.; Li, T.; Li, Z.; Fan, Y. Forest Height Estimation Approach Combining P-Band and X-Band Interferometric SAR Data. Remote Sens. 2022, 14, 3070. https://doi.org/10.3390/rs14133070
- Zhao Lei, Chen Erxue, Li Zengyuan et al. The Improved Three-Step Semi-Empirical Radiometric Terrain Correction Approach for Supervised Classification of PolSAR Data [J]. Remote Sensing, 2022， 14(3):595. DOI:10.3390/rs14030595
- Wan, X.; Li, Z.; Chen, E.; Zhao, L.; Zhang, W.; Xu, K. Forest Aboveground Biomass Estimation Using Multi-Features Extracted by Fitting Vertical Backscattered Power Profile of Tomographic SAR. Remote Sens. 2021, 13, 186. https://doi.org/10.3390/rs13020186
- Ning Liu, Xinwu Li, Xing Peng, Wen Hong, SAR Tomography Based on Atomic Norm Minimization in Urban Areas. Remote Sensing. 2022, 14, 3439.
- Xing Peng, Youjun Wang, Shilin Long, Xiong Pan, Jianjun Zhu, Xinwu Li. Underlying Topography Inversion Using TomoSAR Based on Non-Local Means for an L-Band Airborne Dataset. Remote Sensing, 2021, 13(15), 2926.

- Mor Diama Lo, Matthieu Davy, Laurent Ferro-Famil. Low-Complexity 3D InISAR Imaging Using a Compressive Hardware Device and a Single Receiver. Sensors, 2022, 22 (15), pp.5870. ⟨10.3390/s22155870⟩. ⟨hal-03771179⟩
- Yen-Nhi Ngo, Yue Huang, Dinh Ho Tong Minh, Laurent Ferro-Famil, Ibrahim Fayad, et al.. Tropical forest vertical structure characterization: From GEDI to P-band SAR tomography. IEEE Geoscience and Remote Sensing Letters, IEEE - Institute of Electrical and Electronics Engineers, In press, 19, pp.1-1. ⟨10.1109/LGRS.2022.3208744⟩. ⟨hal-03793062⟩
- Mhamad El Hage, Ludovic Villard, Yue Huang, Laurent Ferro-Famil, Thierry Koleck, et al.. Multicriteria Accuracy Assessment of Digital Elevation Models (DEMs) Produced by Airborne P-Band Polarimetric SAR Tomography in Tropical Rainforests. Remote Sensing, 2022, 14 (17), pp.4173. ⟨10.3390/rs14174173⟩.
- Colette Gelas, Ludovic Villard, Laurent Ferro-Famil, Laurent Polidori, Thierry Koleck, et al.. Multi-Temporal Speckle Filtering of Polarimetric P-Band SAR Data over Dense Tropical Forests: Study Case in French Guiana for the BIOMASS Mission. Remote Sensing, MDPI, 2021, 13 (1)
- Ray Abdo, Laurent Ferro-Famil, Frédéric Boutet, Sophie Allain-Bailhache. Analysis of the Double-Bounce Interaction between a Random Volume and an Underlying Ground, Using a Controlled High-Resolution PolTomoSAR Experiment. Remote Sensing, MDPI, 2021, 13 (4), ⟨10.3390/rs13040636⟩.
- Y. Huang, Q. Zhang, and L. Ferro-Famil, “Forest Height Estimation Using a Single-Pass Airborne L-Band Polarimetric and Interferometric SAR System and Tomographic Techniques,” Remote Sensing, vol. 13, no. 3, p. 487, Jan. 2021, doi: 10.3390/rs13030487.
- Morin D, Planells M, Baghdadi N, Bouvet A, Fayad I, Le Toan T, Mermoz S, Villard L. Improving Heterogeneous Forest Height Maps by Integrating GEDI-Based Forest Height Information in a Multi-Sensor Mapping Process. Remote Sensing. 2022; 14(9):2079. https://doi.org/10.3390/rs14092079
- Emma Bousquet, Arnaud Mialon, Nemesio Rodriguez-Fernandez, Stéphane Mermoz, Yann Kerr. Monitoring post-fire recovery of various vegetation biomes using multi-wavelength satellite remote sensing. Biogeosciences, European Geosciences Union, 2022, 19 (13), pp.3317-3336. ⟨10.5194/bg-19-3317-2022⟩. ⟨hal-03725230⟩
- Salma El Idrissi Essebtey, Ludovic Villard, Pierre Borderies, Thierry Koleck, Benoît Burban, et al.. Long-Term trends of P-band temporal decorrelation over a tropical dense forest-experimental results for the BIOMASS Mission. IEEE Transactions on Geoscience and Remote Sensing, Institute of Electrical and Electronics Engineers, 2022, 60, ⟨10.1109/TGRS.2021.3082395⟩. ⟨hal-03575274⟩
- Yang, H, Ciais, P, Wang, Y, et al. Variations of carbon allocation and turnover time across tropical forests. Global Ecol Biogeogr. 2021; 30: 1271– 1285. https://doi.org/10.1111/geb.13302
- Marie Ballère, Alexandre Bouvet, Stéphane Mermoz, Thuy Le Toan, Thierry Koleck, Caroline Bedeau, Mathilde André, Elodie Forestier, Pierre-Louis Frison, Cédric Lardeux, SAR data for tropical forest disturbance alerts in French Guiana: Benefit over optical imagery, Remote Sensing of Environment, Volume 252, 2021,
- Papathanassiou, K.P. et al. (2021). Forest Applications. In: Hajnsek, I., Desnos, YL. (eds) Polarimetric Synthetic Aperture Radar. Remote Sensing and Digital Image Processing, vol 25. Springer, Cham. https://doi.org/10.1007/978-3-030-56504-6_2

EO Data Delivery

Data access (list all missions and issues if any). NB. in the tables please insert cumulative figures (since July 2020) for no. of scenes of high bit rate data (e.g. S1 100 scenes). If data delivery is low bit rate by ftp, insert “ftp”

ESA Third Party Missions	No. Scenes
1. Sentinel 1	100s
2. GEDI	10s
3. ESA Airborne campaigns	10s
4. UAV SAR	10s
5.	
6.	
Total:	100 s
Issues:	

Chinese EO data	Study Area	No. Scenes
1. CASMSAR	Genhe, Inner Mongolia, China	200+
2.		
3.		
4.		
5.		
6.		
Total:	200+	
Issues:		

European Young scientists contributions in Dragon 5

Name	Institution	Poster title	Contribution
P.-A. BOU	CESBIO & ONERA	3-D SAR imaging of forests from space at higher frequency bands using incoherent bistatic tomography Concepts and validation using the TomoSense campaign	Tomography at higher higher frequencies from space
Y. XI	CSU (China) & CESBIO		BIOMASS DB PolinSAR (Chines-French co-supervision) (arrived in Feb. 2022)
M. BOTTANI	ISAE-SUPAERO & CESBIO		Deforestation monitoring using S1 & S2. Beginning in Nov. 2022

Chinese Young scientists contributions in Dragon 5

Name	Institution	Poster title	Contribution
Kunpeng Xu	IFRIT	Research On Forest Height Extraction Method Based On Multi-band InSAR Data	Presented a forest height estimation approach utilizing the penetration difference between P-band and X-band InSAR data.
Yaxiong Fan	IFRIT	Forest Height Estimation Using Time Series Short-baseline Polarimetric SAR Interferometry Data	Investigated the potential of time series short-baseline PolInSAR data for estimating forest height
Zhiyuan Lin	BUCT	A Temporal Polarization SAR Classification Method Based on Polarimetric-Temporal Feature Selection	PolSAR Time series classification